Inhibition of Heat Shock Protein B8 Alleviates Retinal Dysfunction and Ganglion Cells Loss Via Autophagy Suppression in Mouse Axonal Damage

Feijia Xie,[1,2] Zongyuan Li,[1] Ning Yang,[1] Jiayi Yang,[1] Dihao Hua,[1] Jinyuan Luo,[1] Tao He,[1] and Yiqiao Xing[1]

[1]Eye Center, RenMin Hospital of Wuhan University, Wuhan, Hubei Province, People's Republic of China
[2]State Key Laboratory Cultivation Base, Shandong Provincial Key Laboratory of Ophthalmology, Eye Institute of Shandong First Medical University, Qingdao, Shandong Province, People's Republic of China

Correspondence: Yiqiao Xing, Eye Center, RenMin Hospital of Wuhan University, 238 Jiefang Road, Wuhan 430060, Hubei Province, People's Republic of China;
yiqiao_xing57@whu.edu.cn.
Tao He, Eye Center, RenMin Hospital of Wuhan University, 238 Jiefang Road, Wuhan 430060, Hubei Province, People's Republic of China;
hetao_cb1976@163.com.

TH and YX contributed equally to the work presented here and therefore should be regarded as equivalent authors.

Received: July 18, 2021
Accepted: March 10, 2022
Published: June 27, 2022

Citation: Xie F, Li Z, Yang N, et al. Inhibition of heat shock protein B8 alleviates retinal dysfunction and ganglion cells loss via autophagy suppression in mouse axonal damage. *Invest Ophthalmol Vis Sci.* 2022;63(6):28.
https://doi.org/10.1167/iovs.63.6.28

Purpose. Heat shock protein B8 (HspB8) can be upregulated rapidly in many pathologic processes, but its role in traumatic optic neuropathy remains unclear. In this study, we investigated the involvement of autophagy in the effects of HspB8 by using the optic nerve crush (ONC) model.

Methods. Male C57BL/6J mice were intravitreally injected with recombinant adeno-associated virus type 2 (AAV2-shHspB8 or AAV2-GFP) and subsequently received ONC by a self-closing tweezers. Western blot and immunohistochemistry staining were used to evaluate the expression of HspB8. We conducted retinal flat-mount immunofluorescence to measure the quantities of retinal ganglion cells (RGCs), and full-field flash electroretinogram (ff-ERG) and optomotor response (OMR) were used to evaluate retinal function. The autophagy level was reflected by western blot, immunohistochemistry staining, and transmission electron microscope (TEM) images. We also applied 3-methyladenine (3MA) and rapamycin (Rapa) to regulate autophagy level in optic nerve injury.

Results. ONC stimulated the expression of HspB8. Declines of RGCs and ff-ERG b-wave amplitudes resulting from ONC can be alleviated by HspB8 downregulation. Increased autophagy activity after ONC was observed; however, this change can be reversed by intravitreal injection of AAV2-shHspB8. Furthermore, application of autophagy inhibitor 3MA had the same neuroprotective effects as AAV2-shHspB8, as illustrated by ff-ERG and quantities of RGCs. Also, protection of AAV2-shHspB8 was compromised by the autophagy activator Rapa.

Conclusions. Inhibition of HspB8 in mice optic nerve injury had neuroprotective effects, which may be derived from its downregulation of autophagy.

Keywords: heat shock protein B8, retinal ganglion cells, electroretinogram, autophagy, neuroprotection

As an integral part of the central nervous system, the optic nerve (ON) is often used for research on neuroprotection and regeneration of the central nervous system by virtue of its accessibility in animal models and functional detection.[1,2] Similar to the pathological process of glaucomatous neurodegeneration, axonal damage of the ON is also characterized by progressive loss of retinal ganglion cells (RGCs) and ON fibers, leading to severe and irreversible visual damage.[3] Clinical prognosis is strongly associated with the survival of RGCs,[4] and it has been suggested that the degeneration and death of RGCs is caused in two ways: primary and secondary.[5,6] Hence, it is crucial to explore treatment to protect RGCs and maintain the integrity of the axons projecting to the brain, in addition to protecting RGCs and glial cells that are unaffected or only partially affected by primary damage from secondary degeneration.[7]

As a member of the ubiquitous small heat shock protein family, heat shock protein B8 (HspB8) can be upregulated promptly after various kinds of stress.[8] By participating in proteolytic processes, including proteasome and autophagy, HspB8 can facilitate the degradation of terminally misfolded proteins.[9,10] HspB8 can also combine with Bcl-2–associated athanogene 3 (BAG3) to form the HspB8–BAG3 complex, which engages in autophagy stimulation and plays a decisive role in various neurodegenerative diseases.[11,12] The dual effects of HspB8 on cell death seem to vary with cell type and extent of expression.[13–15]

Autophagy is an important physiological cellular process that promotes the degradation and recycling of cellular components to maintain homeostasis.[16] Misfolded proteins and damaged organelles cannot be reduced through cell division in neurons, which makes autophagy even more necessary in the nervous system.[17] The role of autophagy

in axonal damage remains unclear, as some research has shown that inhibition of autophagy alleviates axonal degeneration after ON injury,[18] but another study reported conflicting results.[19]

In this study, we explored the impacts of HspB8 on visual function and RGCs survival rate, as well as the role of autophagy and its participation in the effects of HspB8 by using the optic nerve crush (ONC) model in mice.

Materials and Methods

Recombination of Adeno-Associated Virus Type 2 Vector

An adeno-associated virus type 2 (AAV2) vector (GV478, U6-MCS-CAG-EGFP; Shanghai Genechem Co., Ltd., Shanghai, China) containing AAV2-scrambled HspB8 (shHspB8; U6-MCS-CAG-EGFP-HspB8-shRNA, targeting sequence 5′-CCGGAAGAGCTGATGGTAA) and AAV2-green fluorescent protein (GFP; empty GV478 vector without HspB8-shRNA, U6-MCS-CAG-EGFP) was constructed as an HspB8 silencing vector and negative control, respectively. These two highly purified vectors both contain the enhanced green fluorescent protein (EGFP) gene driven by the CAG promoter. AAV2-shHspB8 (1.58×10^{12} viral genomes vg/mL) and AAV2-GFP (1.95×10^{12} vg/mL) were stocked at −80°C for follow-up use.

Intravitreal Injection

As previously described,[20] precise intravitreal injection was accomplished with a programmable nanoliter injector (Nanoject III, Drummond Scientific Company, Broomall, PA, USA) and pulled glass micropipettes using a dual-stage glass micropipette puller (Narishige Scientific Instrument Lab, Setagaya City, Japan). After exposing the superior temporal side of anesthetized mice eyes sufficiently while avoiding blood vessels, a slow injection into the vitreous cavity was carefully performed through the sclera 1 to 2 mm posterior to the corneoscleral limbus. One minute later, the micropipette was withdrawn to prevent leakage, and antibiotic ophthalmic ointment was applied to avoid infection. The injection solution (1 µL) was comprised of AAV2-shHspB8 and AAV2-GFP vectors (1.58×10^{12} vg/mL and 1.95×10^{12} vg/mL, respectively). We injected 3-methyladenine (3MA; 1 µL, 50 mM; MedChemExpress, Monmouth Junction, NJ, USA) or rapamycin (Rapa; 1 µL, 1 mM, MedChemExpress, NJ, USA) right before ONC. The 3MA was dissolved in phosphate-buffered saline (PBS); the Rapa was dissolved in dimethyl sulfoxide (DMSO) and diluted in 5% Tween 80 (Sigma-Aldrich, St. Louis, MO, USA), 40% polyethylene glycol 400, and 45% 0.9% NaCl. Both drugs were prepared just before administration. Four weeks after injection of the vector, mice were euthanized for further examinations. The doses and timing were selected based on similar studies.[18,21–23] A timeline of all animal procedures is shown in Figure 1.

Animal Model of ONC

Male C57BL/6J mice (8 weeks) provided by the Laboratory Animal Center of Wuhan University were kept in an air-conditioned barrier system with sufficient food and water (room temperature, 23° ± 2°C; 12-hour light/dark cycle). After 7 days of acclimation, mice were randomly assigned to interventions. All animal procedures were conducted in accordance with National Institutes of Health guidelines and conformed to the ARVO Statement for the Use of Animals in Ophthalmic and Vision Research. Mice with lens damage, postoperative bleeding, or eye infection were removed.

After the mice were anesthetized by intraperitoneal injection of pentobarbital sodium, an incision was made at the temporal side of the mice conjunctiva. By using forceps, a blunt dissection of the orbital fat and muscle was made toward the back of the eye to expose the retrobulbar ON. The ON was crushed with self-closing Dumont Tweezers (Electron Microscopy Sciences, Hatfield, PA, USA) at about 2 mm posterior to the globe for 8 seconds. Special attention was paid to avoiding the surrounding blood vessels. After the operation, the antibiotic ophthalmic ointment was applied to avoid infection, and the animal was resuscitated on a warming pad.

Western Blot

Retinas were quickly obtained over ice and immersed immediately in a homogenizer preloaded with radioimmunoprecipitation assay lysis buffer containing a 50-mM tris–HCl, 150-mM NaCl, 1% NP-40, 0.1% sodium dodecyl sulfate (SDS), 0.5% sodium deoxycholate, 1-mM EDTA, and 1-mM phenylmethylsulfonyl fluoride (PMSF) protease inhibitor cocktail. Supernatants were collected after homogenization and centrifugation, and total protein concentrations

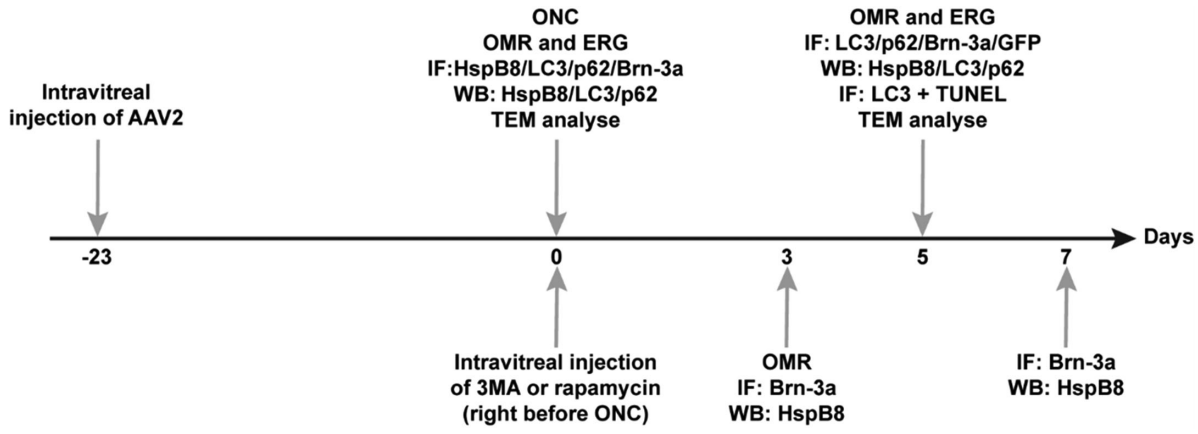

Figure 1. Experimental timeline. IF, Immunofluorescent staining; WB, western blot analysis; TEM: transmission electron microscopy.

Investigative Ophthalmology & Visual Science

were measured by a bicinchoninic acid protein assay kit. After separation in 12% SDS–polyacrylamide gel, proteins were transferred to a polyvinylidene fluoride membrane. Later, the membrane was blocked with 5% nonfat milk and 0.1% Tween-20 in tris-buffered saline (TBS-T) for 2 hours at room temperature, then incubated with the HspB8 (#3059, rabbit mAb, 1:500; Cell Signaling Technology, Boston, MA, USA), light chain 3B (LC3B; #3868S, rabbit mAb, 1:1000; Cell Signaling Technology), p62 (#23214S, rabbit mAb, 1:1000; Cell Signaling Technology), and glyceraldehyde 3-phosphate dehydrogenase (GAPDH; #GB11002, rabbit mAb, 1:1000; Servicebio, Wuhan, China) overnight at 4°C. GAPDH was determined to be the housekeeping protein. After washing in TBS-T solution, the membrane was incubated with horseradish peroxidase-labeled goat anti-rabbit immunoglobulin (IgG; Servicebio) at room temperature for 2 hours. The immunoreactive bands were developed using an enhanced chemiluminescence substrate kit (Biosharp, Anhui, China) and observed using the ChemiDoc Touch Imaging System (Bio-Rad, Hercules, CA, USA). Protein levels were analyzed using ImageJ software (National Institutes of Health, Bethesda, MD, USA). To estimate the molecular weight of proteins, a prestained marker (Servicebio) was used.

Retinal Flat-Mount Immunofluorescence

Extracted eyes were fixed in 4% paraformaldehyde for 30 minutes, then retinas were separated and blocked at 4°C overnight with PBS containing 5% bovine serum albumin (GoodbioTechnology, Wuhan, China) and 0.5% Triton X-100. After the retinas were incubated with Brn3a (#411003, rabbit pAb, 1:1000; Synaptic Systems, Göttingen, Germany) for 48 hours and gently rinsed in PBS three times, they were incubated with Alexa Fluor 594 (#705-585-147; Jackson ImmunoResearch Labs, West Grove, PA, USA) for 2 hours. Four radial incisions were made to form retinas into a petal shape. Three areas of each retinal petal, located 0.5, 1.6, and 2.7 mm from the optic disc (Fig. 2C) for a total of 12 fields, were selected and photographed by a fluorescence microscope (BX51; Olympus, Tokyo, Japan). Surviving RGCs were marked using the ImageJ Multi-point Tool and counted using ImageJ software. The number of surviving RGCs was compared with the control group to determine RGCs survival.

Scotopic Full-Field Flash Electroretinogram

After being dark-adapted for 12 hours, mice were anesthetized intraperitoneally with pentobarbital sodium under dim red light. Phenylephrine HCl (0.5%) and tropicamide (0.5%) were used to dilate pupils, and 1% sodium hyaluronate was used to lubricate and hydrate the cornea. Gold-plated wire loops were gently and vertically placed on the center of corneal surfaces as recording electrodes, and stainless steel needle electrodes were inserted into the skin between the two ears and into the tail to serve as reference and ground leads, respectively. After turning off the dim red light, a Ganzfeld full-field stimulator and RetiMINER visual electrophysiological apparatus (Chongqing IRC Medical Equipment Co., Ltd., Chongqing, China) were used to record responses of white flashes (with luminance increased sequentially: 0.001, 0.003, 0.01, 0.03, 0.10, 0.30, 1.00, 3.00, and 10.00 cd·s/m^2) in scotopic full-field flash electroretinograms (ff-ERGs). A series of non-erratic high-frequency wavelets on the ascending side of the b-wave were recorded as oscillatory potentials (OPs). After the mice adapted to the green background (25 cd·s/m^2) for 8 minutes, they were given a green light stimulation (10.0 cd·s/m^2); the amplitudes relative to the baselines of the negative peak following the b-wave were measured as photopic negative responses (PhNRs). Mice were placed on a heating pad to maintain their body temperature during the entire examination. The following variables were under strict control when all ERG data were collected: depth of anesthesia, room temperature, mouse weight, and distance between eyes and the stimulator.

Optomotor Response

Based on previous research,[24] mice were placed on the platform in the center of the device after dark adaptation for 4 hours, and rotating gratings with constant contrast and velocity were displayed on the four screens around the mice. When a grating was perceived, the mouse usually stopped moving its body and would begin to track the grating with reflexive head movements in concert with the rotation. This is an image stabilization reflex that compensates for the offset of the visual scene. Optomotor responses (OMRs) were recorded using MATLAB software (MathWorks, Natick, MA, USA) and a virtual optomotor system that we assembled. When the OMR device is running, the higher the grating spatial frequency is the more difficult it is to distinguish and thus be followed by mice and produce OMRs afterward. The highest grating spatial frequency (cycles/degrees) that induced OMRs was used as visual acuity to measure the visual function of mice.

Cryosection Immunofluorescent Staining

The procedure has been described elsewhere.[25] Eyes were extracted quickly and fixed in 4% paraformaldehyde for 1 hour before the anterior segments were removed. After they were dehydrated at 4°C in 10%, 20%, and 30% sucrose for 2 hours, 2 hours, and 8 hours, respectively, the retinas were embedded in optimum cutting temperature compound (Sakura Finetek USA, Torrance, CA, USA) and sectioned (14 °m) using a freezing microtome (Leica, Wetzlar, Germany). The retinal slices were blocked at room temperature for 2 hours with 5% bovine serum albumin and 0.5% Triton X-100 in PBS, then immunostained with primary antibodies as follows: HspB8 (Cell Signaling Technology), anti-GFP antibody (ab10145, 1:1000; MilliporeSigma, Burlington, MA, USA), LC3B (Cell Signaling Technology), and p62 (Cell Signaling Technology). Cryosections were incubated with Alexa Fluor 488 (#711-545-152, 1:500; Jackson ImmunoResearch Labs) and Alexa Fluor 594 (Jackson ImmunoResearch Labs). Finally, 4′,6-diamidino-2-phenylindole (DAPI) was used to label the cell nucleus of the retina. The sections were observed and photographed using an Olympus FV1200 confocal laser scanning microscope.

Transmission Electron Microscope

Blocks of 1-mm^3 of retinal tissue were fixed for 4 hours at 4°C in 3% glutaraldehyde (pH 7.4) and washed with 0.1-M phosphate buffer (pH 7.2) for three times, then fixed again in osmic acid for 1 hour; after that, tissue was dehydrated by acetone and embedded in Epon-Araldite resin (18030, Ted Pella Inc., Redding, CA, USA). By using the Leica EM UC6 Ultramicrotone, semi-thin sections (1 °m) were made into ultra-thin sections (70 nm), which were counterstained with

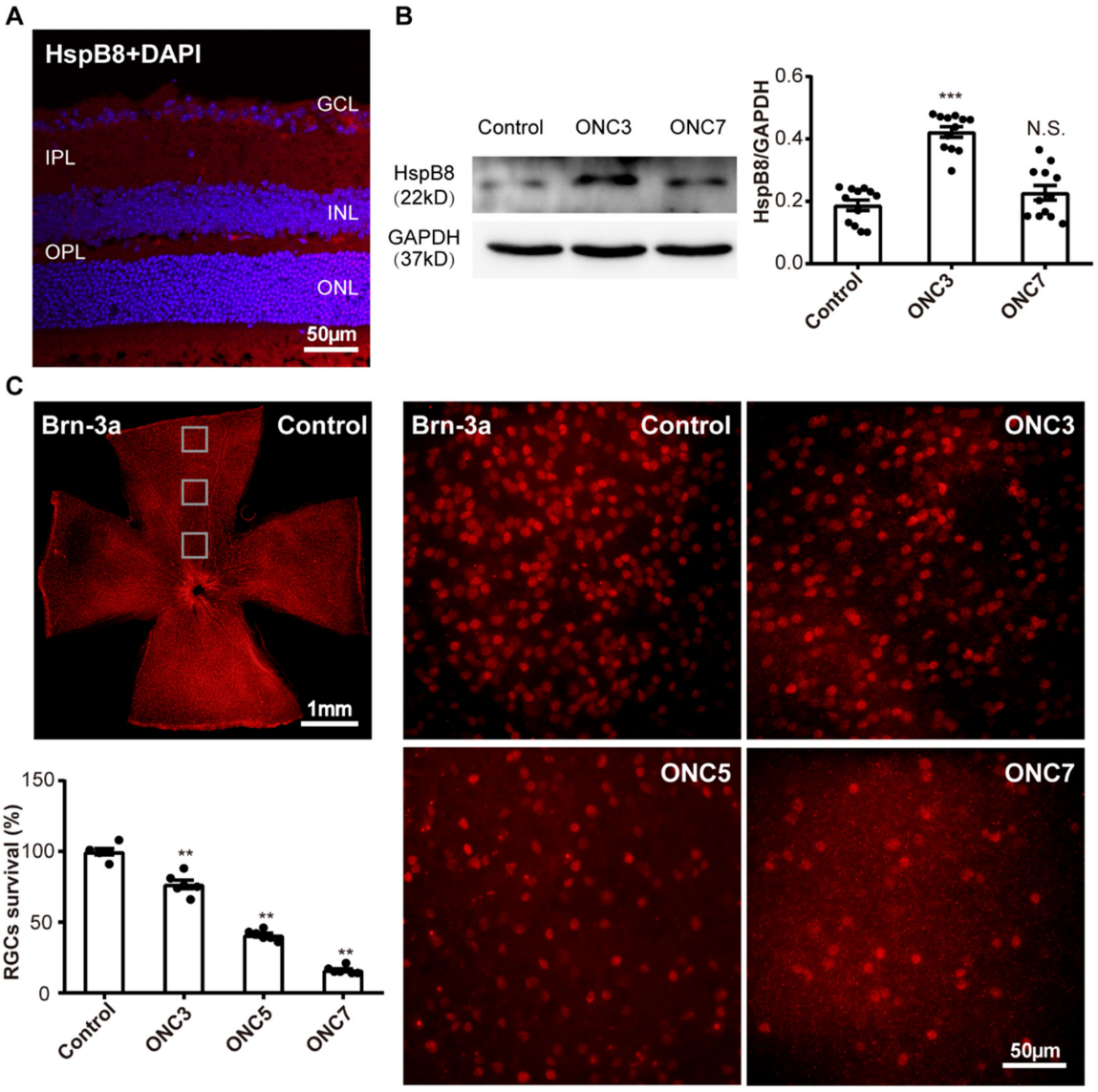

Figure 2. RGCs loss and HspB8 expression changes after ONC. (**A**) Immunofluorescent staining of HspB8 (*red*) in normal retinal slices. (**B**) Western blot revealed that, compared with the control group (0.19 ± 0.02), HspB8/GAPDH increased in the ONC3 group (0.42 ± 0.02, $P < 0.0001$), and there was no significant difference in the ONC7 group (0.23 ± 0.02, $P = 0.8998$); $n = 12$. (**C**) Immunofluorescent staining of Brn3a. RGCs survival rates continued to decrease in the ONC3 group (76.62% ± 3.05%, $P = 0.0022$), ONC5 group (40.93% ± 1.32%, $P = 0.0022$), and ONC7 group (16.00% ± 1.12%, $P = 0.0022$) compared with the control group (100.00% ± 2.30%). The second areas on the retinal flat-mounts of each group were selected as example images ($n = 6$). All data are presented as mean ± SEM. ONC3, ONC5, and ONC7 indicate 3, 5, and 7 days after ONC.

3% uranyl acetate and 0.3% lead citrate. Observation and photography were carried out using a transmission electron microscope (JEM-1230; JEOL, Tokyo, Japan).

TdT-Mediated dUTP Nick-End Labeling Staining Assay

To explore the relationship between apoptosis and autophagy, a TdT-mediated dUTP nick-end labeling (TUNEL) assay kit (Beyotime Biotechnology, Shanghai, China) was used to detect apoptotic cells before retinal sections were immunostained by LC3, secondary antibody Alexa Fluor 647 (ANT032, donkey anti-rabbit IgG, 1:1000; AntGene, Wuhan, China) and DAPI as described previously. Slices were washed three times in PBS for 10 minutes, permeabilized with 0.5% Triton X-100 in PBS for 5 minutes at room temperature, and washed twice in PBS for 10 minutes. The slices were incubated in TUNEL detection solution for 1 hour at 37°C in a dark place and finally washed three times in PBS for 10 minutes. The TUNEL detection solution was freshly prepared from terminal deoxynucleotidyl transferase and a fluorescent marking reagent (1:9, v/v) in a dark place. Slices were examined by confocal laser scanning microscope (Olympus FV1200).

Statistics

Data were analyzed by Prism 8.0 (GraphPad Software, San Diego, CA, USA) and expressed as means ± SEM. Differ-

Investigative Ophthalmology & Visual Science

ences between groups were analyzed by Student's *t*-test or one-way ANOVA followed by Tukey's post hoc test for multiple comparisons. $P < 0.05$ was considered to be significant ($^{*}P < 0.05$, $^{**}P < 0.01$, $^{***}P < 0.001$).

Results

ONC Induced RGCs Loss and HspB8 Dynamic Changes

Immunofluorescence of normal retinal sections demonstrated that HspB8 was distributed in the inner plexiform layer (IPL), inner nuclear layer (INL), outer plexiform layer (OPL), and even in the internal segment layer of photoreceptors, but it is most obvious in the ganglion cell layer (GCL) (Fig. 2A). A marked increase in HspB8 was observed 3 days after ONC, but it soon declined to a nearly normal level on the seventh day (Fig. 2B), whereas RGCs decreased continuously after ONC (Fig. 2C). These results indicate that HspB8 may be involved in RGCs loss following ONC.

Retinal Function Receded After ONC

The ff-ERGs and OMRs were performed after ONC to investigate visual impairments. Compared with the control group, the ONC5 group (5 days after ONC) had prolonged latency, decreased amplitudes of b-waves (Figs. 3A, 3D; Table; see also Fig. 5F), decreased amplitudes of PhNRs (Figs. 3B, 3C),

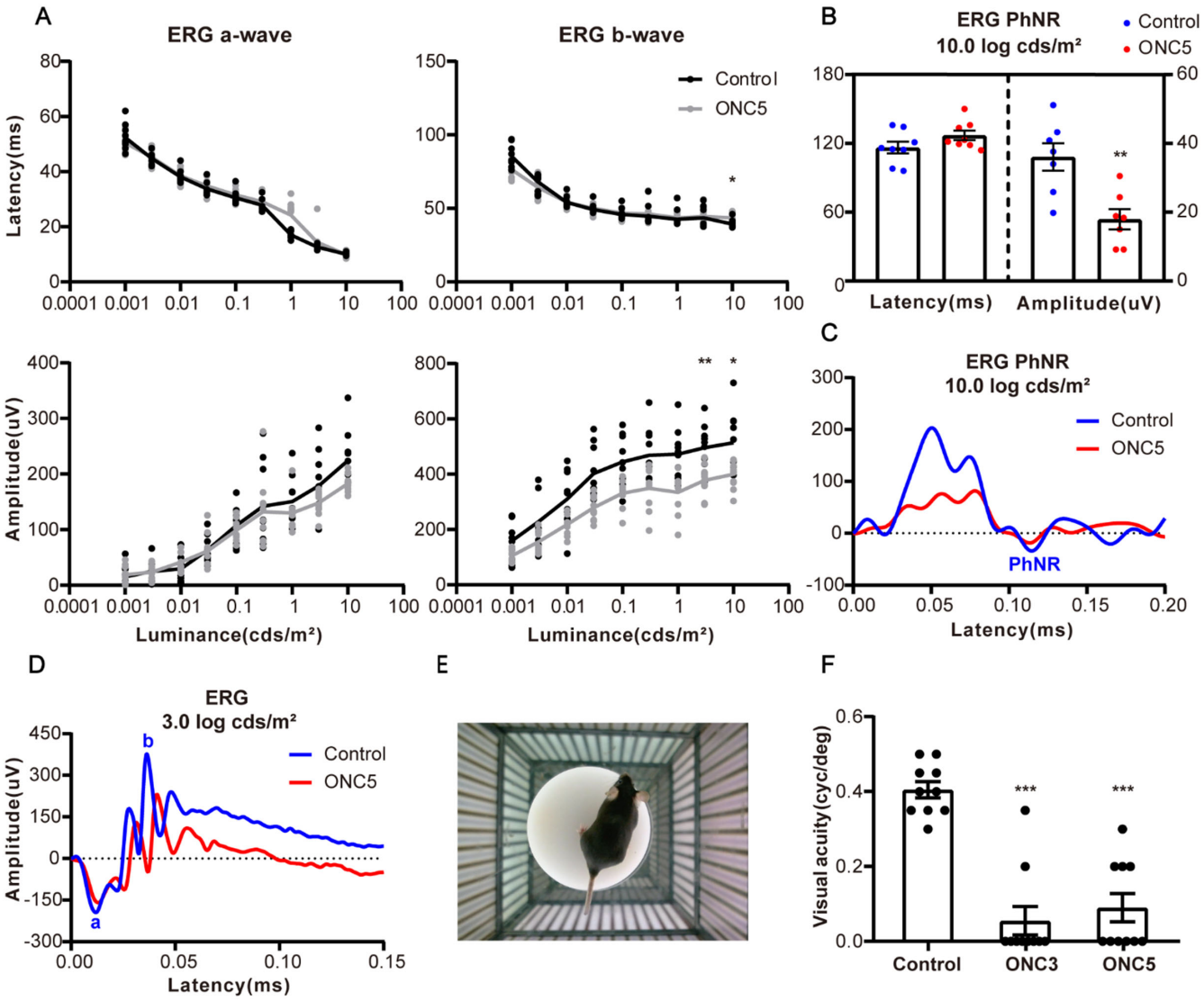

Figure 3. Characteristics of ff-ERG and OMR following ONC. (**A**) Latencies shortened and amplitudes increased gradually along with the increasing luminance of the flash lights. There were lengthened latencies (10.0 cd·s/m^2) and decreased amplitudes (3.0 and 10.0 cd·s/m^2) of b-waves and unaffected latency and amplitudes of a-waves in the ONC5 group compared with the control group ($P = 0.0168$, $P = 0.0062$, $P = 0.0383$, $P = 0.4336$, $P = 0.1189$, and $P > 0.9999$, respectively; $n = 10$). The data are shown in the Table. (**B**) For PhNRs, the ONC5 group had a lower amplitude (17.94 ± 2.94 µV; $P = 0.0022$) but a not significantly different latency (127.00 ± 4.22 ms; $P = 0.2956$) compared with the control group (36.09 ± 4.01 µV, 116.40 ± 5.16 ms); $n = 7$. (**C**) Representative PhNRs in the control group and ONC5 group. (**D**) Example scotopic ERG waves of the control group and ONC5 group. (**E**) Detection of OMRs by the virtual optomotor system. (**F**) Both the ONC3 group (0.06 ± 0.04 cyc/deg) and the ONC5 group (0.09 ± 0.04 cyc/deg) had significantly reduced visual acuities compared with the control group (0.41 ± 0.02 cyc/deg) ($P = 0.0001$ and $P = 0.0006$, respectively; $n = 10$). All data are presented as mean ± SEM.

Investigative Ophthalmology & Visual Science

Table. ERG Characteristics in This Study

	Mean ± SEM								
	Control	**ONC5**	**AAV2-shHspB8 + ONC5**	**AAV2-GFP + ONC5**	**AAV2-shHspB8**	**ONC5 + 3MA**	**ONC5 + Rapa**	**ONC5 + DMSO**	**AAV2-shHspB8 + ONC5 + Rapa**
a-wave									
Latency of 10.0 (ms)	10.05 ± 0.14	9.90 ± 0.25	10.05 ± 0.17	9.80 ± 0.20	10.35 ± 0.33	10.35 ± 0.21	9.95 ± 0.19	10.20 ± 0.31	9.95 ± 0.35
Amplitude of 3.0 (μV)	178.80 ± 17.75	148.10 ± 6.54	209.30 ± 23.93	165.00 ± 8.70	183.40 ± 8.38	234.80 ± 9.87	280.80 ± 19.20	172.90 ± 6.53	156.80 ± 12.86
Amplitude of 10.0 (μV)	224.10 ± 15.78	182.90 ± 5.63	230.60 ± 16.92	187.00 ± 14.57	210.40 ± 11.64	261.30 ± 12.25	306.30 ± 12.64	219.60 ± 12.92	173.10 ± 15.79
b-wave									
Latency of 10.0 (ms)	39.25 ± 0.86	43.50 ± 0.93	41.50 ± 0.47	39.65 ± 0.46	40.85 ± 1.34	43.95 ± 0.89	40.55 ± 2.52	41.90 ± 1.63	43.35 ± 2.21
Amplitude of 3.0 (μV)	495.80 ± 25.53	378.00 ± 17.39	594.70 ± 38.21	380.50 ± 25.67	535.50 ± 10.80	591.80 ± 29.69	585.50 ± 28.21	436.40 ± 24.89	342.70 ± 32.53
Amplitude of 10.0 (μV)	513.50 ± 33.93	399.60 ± 16.05	567.00 ± 26.74	407.40 ± 19.85	551.00 ± 11.96	570.80 ± 36.38	576.60 ± 26.82	421.10 ± 23.49	357.40 ± 21.95
OPs wave									
Amplitude of 3.0 (μV)	361.70 ± 8.98	336.60 ± 16.96	309.40 ± 8.24	312.40 ± 17.90	344.40 ± 18.31	385.30 ± 22.75	523.70 ± 40.14	393.50 ± 34.38	318.00 ± 37.10

Data were obtained from 10 independent experiments; 10.0 indicates 10.0 log cd·s/m^2, and 3.0 indicates 3.0 log cd·s/m^2.

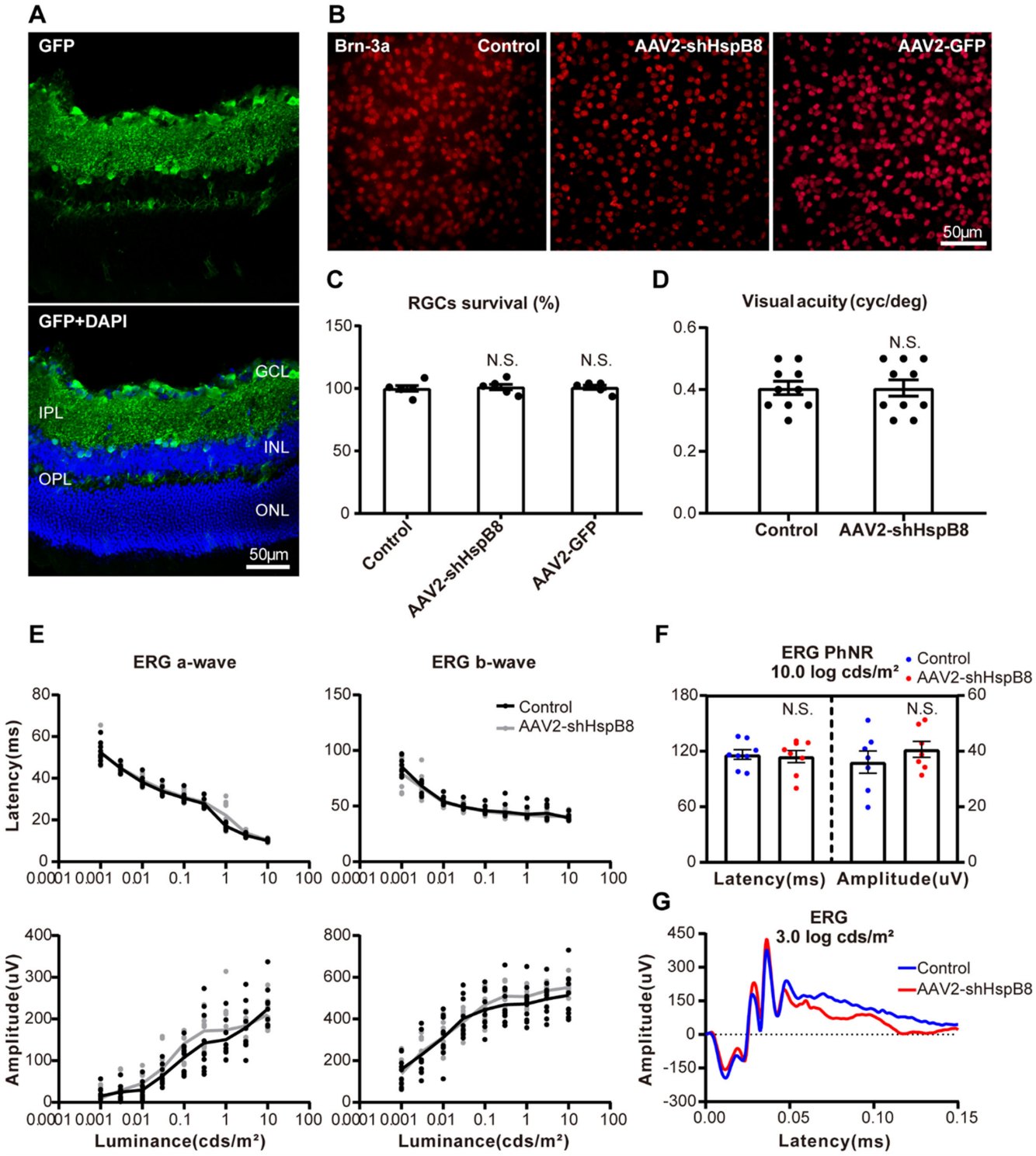

Figure 4. Intravitreal injection of AAV2 had no impact on RGCs survival and visual function. (**A**) GFP immunofluorescent staining of retinal section in the AAV2-shHspB8 group. (**B**) Representative pictures of retinal flat-mounts stained by Brn3a in the control group, AAV2-shHspB8 group, and AAV2-GFP group. (**C**) RGCs survival rates showed no evident decrease in the AAV2-shHspB8 group (101.20% ± 2.18%) or AAV2-GFP group (100.90% ± 1.63%) compared with the control group (100.00% ± 2.30%) ($P = 0.8925$ and $P = 0.9367$, respectively; $n = 6$). (**D**) Visual acuity appeared to be unaffected by intravitreal injection of AAV2-shHspB8 (0.41 ± 0.03 cyc/deg) compared with the control group (0.41 ± 0.02 cyc/deg) ($P > 0.9999$; $n = 10$). (**E**) No differences in latencies were statistically significant (10.0 cd·s/m^2), nor were differences in amplitudes (3.0 and 10.0 cd·s/m^2, respectively) of a-waves ($P > 0.9999$, $P = 0.9989$, and $P = 0.9341$, respectively) and b-waves ($P > 0.9999$, $P = 0.5400$, and $P = 0.7851$, respectively) in the control group and the AAV2-shHspB8 group ($n = 10$). Data are presented in the Table. (**F**) Neither the latency nor the amplitude of PhNRs showed significant differences between the AAV2-shHspB8 group (114.20 ± 6.51 ms, 40.64 ± 2.89 μV) and the control group (116.40 ± 5.16 ms, 36.09 ± 4.01 μV) ($P = 0.9416$ and $P = 0.5336$, respectively; $n = 7$). (**G**) Example ff-ERG waves of the control group and AAV2-shHspB8 group. All data are presented as mean ± SEM.

Investigative Ophthalmology & Visual Science

and distinctly damaged visual acuity in OMRs (Fig. 3F). Interestingly, visual acuity did not decline synchronically with the RGCs survival rate but had already approached almost zero in the ONC3 group (3 days after ONC). There were no significant differences in latency, a-wave amplitudes, or the amplitudes of OPs between the control group and the ONC5 group (Figs. 3A, 3D; Table; see also Fig. 5F).

Intravitreal Injection of AAV2-shHspB8 Had No Effect on RGCs Survival Rate and Retinal Function

To evaluate the efficiency of AAV2-U6-MCS-CAG-EGFP-HspB8-shRNA (AAV2-shHspB8) transfection, GFP immunofluorescent staining was performed in retinal slices 4 weeks after the intravitreal injection. Figure 4A shows that the GFP was distributed mainly in the GCL, IPL, and INL and was weaker in the OPL and outer nuclear layer (ONL). Compared with the control group, RGCs survival rates in both the AAV2-U6-MCS-CAG-EGFP (AAV2-GFP) group and AAV2-shHspB8 group showed no evident reductions (Figs. 4B, 4C). No significant differences were found in visual acuity (Fig. 4D), latencies, or the amplitudes of a-waves, b-waves, and PhNRs (Figs. 4E–4G, Fig. 5F) between the control group and the AAV2-shHspB8 group. Amplitudes of OPs in these two groups also did not seem to differ (Fig. 5H). These results confirm the lack of an effect of AAV2 intravitreal injections on retinal function and quantity of RGCs.

Downregulation of HspB8 Alleviated RGCs Loss and Retinal Dysfunction Caused by ONC

Western blot indicated that, whether or not ONC was performed, protein levels of HspB8 were reduced by intravitreal injection of AAV2-shHspB8 (Fig. 5A), which also led to maintaining RGCs quantity (Figs. 5B, 5C) and the amplitudes of b-waves (Figs. 5E–5G). Although visual acuity in the AAV2-shHspB8 + ONC5 group increased slightly compared to the ONC5 group and the AAV2-GFP + ONC5 group, none of these differences was statistically significant (Fig. 5D). No differences were observed in the amplitudes of OPs (Fig. 5H). These results suggest that intravitreal injection of AAV2-shHspB8 protected the retina from ON injury by downregulating HspB8.

ONC-Induced Autophagy Was Inhibited by AAV2-shHspB8

As an ingredient and a substrate of autophagy, respectively,[26,27] microtubule-associated protein LC3 and sequestosome 1 (SQSTM1/p62) are often used as markers to measure autophagy level. We determined LC3II/LC3I ratios and p62 levels to further explore the mechanism underlying the neuroprotection of AAV2-shHspB8. Consistent with a previous study,[18] our western blot results indicated raised LC3II/LC3I ratios and p62 levels after ONC (Fig. 6A), and immunofluorescent staining had a similar tendency; moreover, the distribution of LC3 changed from a diffuse pattern to a punctate pattern (Fig. 6B). All of these results indicate that autophagy can be induced by ONC, a finding that has been reported by several previous studies.[18,28,29] Western blot and immunofluorescent staining also suggested that the LC3I to LC3II transformation was repressed and p62 level was enhanced by AAV2-shHspB8 injection in mice with ONC injury (Figs. 6A, 6B), which implied autophagy inhibition of HspB8 silencing. After ONC, swelling organelles, karyopyknosis in apoptosis cells, and, most importantly, increased autolysosomes in RGCs and nerve fibers were detected in transmission electron microscope images, whereas the application of AAV2-shHspB8 reduced these changes and maintained subcellular structures (Fig. 7). These results support the hypothesis that the neuroprotection of AAV2-shHspB8 may stem from its limiting overactive autophagy.

Autophagy Suppression may be the Protective Mechanism of AAV2-shHspB8 in Retina

Autophagy inhibitor 3MA and activator Rapa were used to clarify the contribution of autophagy inhibition to the protective effects of AAV2-shHspB8. The 3MA maintained ff-ERG performance and the quantity of RGCs after ONC just like AAV2-shHspB8 did; however, Rapa aggravated RGCs death, not only in mice undergoing ONC but also in mice injected AAV2-shHspB8 after ONC, which means that autophagy plays a critical role in the retina and its acceleration compromises the neuroprotection of AAV2-shHspB8 (Figs. 8A, 8B, 8D–8F). Surprisingly, the ONC5 + Rapa group had ascending amplitudes of a- and b-waves, in contrast to the RGCs survival rate (Figs. 8D–8F). This might result from the multiple pathway effects of Rapa. OMRs aligned with RGCs survival rates, as the differences appeared to be insignificant (Fig. 8C). There were no significant differences among these six groups in the latencies of a- and b-waves (data shown in Supplementary Material S1) and the amplitudes of OPs (Fig. 8G).

As shown in the retinal section images in Figure 9A, in those groups that underwent ONC the application of 3MA reduced LC3 and improved p62, whereas Rapa had an opposite effect and eliminated the autophagy suppression effects of AAV2-shHspB8 on LC3 and p62. These findings confirm the inhibition and activation impact of autophagy by 3MA and rapamycin, respectively. Taken together, we may draw a conclusion that downregulation of HspB8 protected RGCs and retinal function against ON insult through autophagy suppression.

To explore the relevance between autophagy and apoptosis of RGCs, retinas were stained by TUNEL, LC3, and DAPI 5 days after ONC. As Figure 9B shows, some TUNEL-positive cells had bright LC3-stained puncta (white arrows); however, there was also a TUNEL-positive cell that did not have an obvious distribution of LC3 (Fig. 9B, white arrowhead). Thus, we can conclude that RGCs apoptosis in ONC injury may be partly attributed to hyperactive autophagy.

Discussion

It is well established that activation of autophagy is a prominent feature of optic axonal degeneration,[18,19] and it plays a key role in maintaining axonal homeostasis.[30] Previous research has suggested that HspB8 participates in autophagy activation and becomes involved in various neuropathology conditions.[11,12] Indeed, research has only begun to investigate autophagy and HspB8 in the visual system, and their roles remain a mystery. Here, we have illustrated the effects of HspB8 in optic axonal damage and its relationship with autophagy.

Previous studies have reported that autophagy occurs mainly in RGCs and Müller cells after ONC.[31] Although

Investigative Ophthalmology & Visual Science

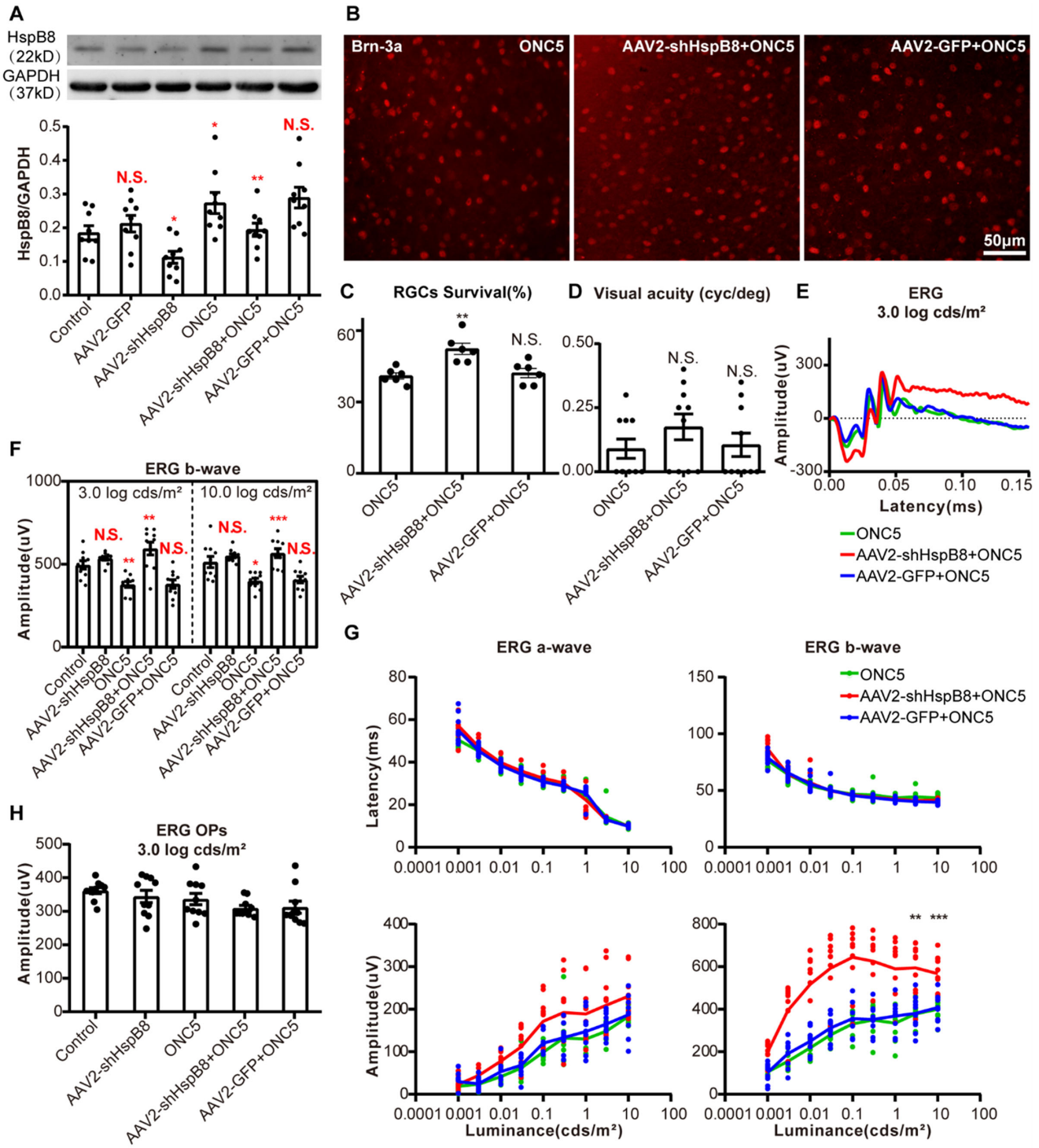

Figure 5. Silencing of HspB8 protected RGCs and retinal function. (**A**) The AAV2-shHspB8 group had lower HspB8 protein levels (0.11 ± 0.02) compared with the control group (0.19 ± 0.02) ($P = 0.0436$), as did the AAV2-shHspB8 + ONC5 group (0.19 ± 0.02) compared with the AAV2-GFP + ONC5 group (0.29 ± 0.03) ($P = 0.0089$). Consistent with previous results, the ONC5 group had increased HspB8 levels (0.27 ± 0.03) compared with the control group ($P = 0.0148$). No significant differences were found for the AAV2-GFP group (0.21 ± 0.02; $P = 0.4383$) compared with the control group or for the AAV2-GFP + ONC5 group compared with the ONC5 group ($P = 0.6461$); $n = 9$. (**B**) Representative RGCs immunofluorescent images stained by Brn3a: ONC5 group, AAV2-shHspB8 + ONC5 group, and AAV2-GFP + ONC5 group. (**C**) The RGCs survival rate of the AAV2-shHspB8 + ONC5 group was higher (52.32% ± 2.38%) than that for the AAV2-GFP + ONC5 group (42.14% ± 1.95%) ($P = 0.0040$), whereas the AAV2-GFP + ONC5 group showed no significant change compared with the ONC5 group (40.93% ± 1.32%) ($P > 0.9999$; $n = 6$). (**D**) There were no significant differences among the visual acuities of the ONC5 group, AAV2-shHspB8 + ONC5 group, and AAV2-GFP + ONC5 group ($P = 0.3672$; $n = 10$). (**E**) Typical ERG waves indicated that the AAV2-shHspB8 + ONC5 group had enhanced b-wave amplitudes compared with the other two groups. (**F**) The b-wave amplitudes at 3.0 and 10.0 cd·s/m^2 ($n = 10$). (**G**) The a- and b-wave latencies demonstrated no significant changes among the three groups. The AAV2-shHspB8 + ONC5 group had higher b-wave amplitudes than those in the AAV2-GFP + ONC5 group at 3.0 and 10.0 cd·s/m^2 ($P = 0.0011$ and $P = 0.0007$, respectively), whereas no difference was observed between the AAV2-GFP + ONC5 group and the ONC5 group ($P > 0.9999$ and $P = 0.9968$, respectively). Although similar changes were found in the a-wave amplitudes, none of these differences was statistically significant. Data are shown in the Table ($n = 10$). (**H**) Amplitudes of OPs at 3.0 cd·s/m^2 ($n = 10$). Data are shown in the Table. All data are presented as mean ± SEM.

Investigative Ophthalmology & Visual Science

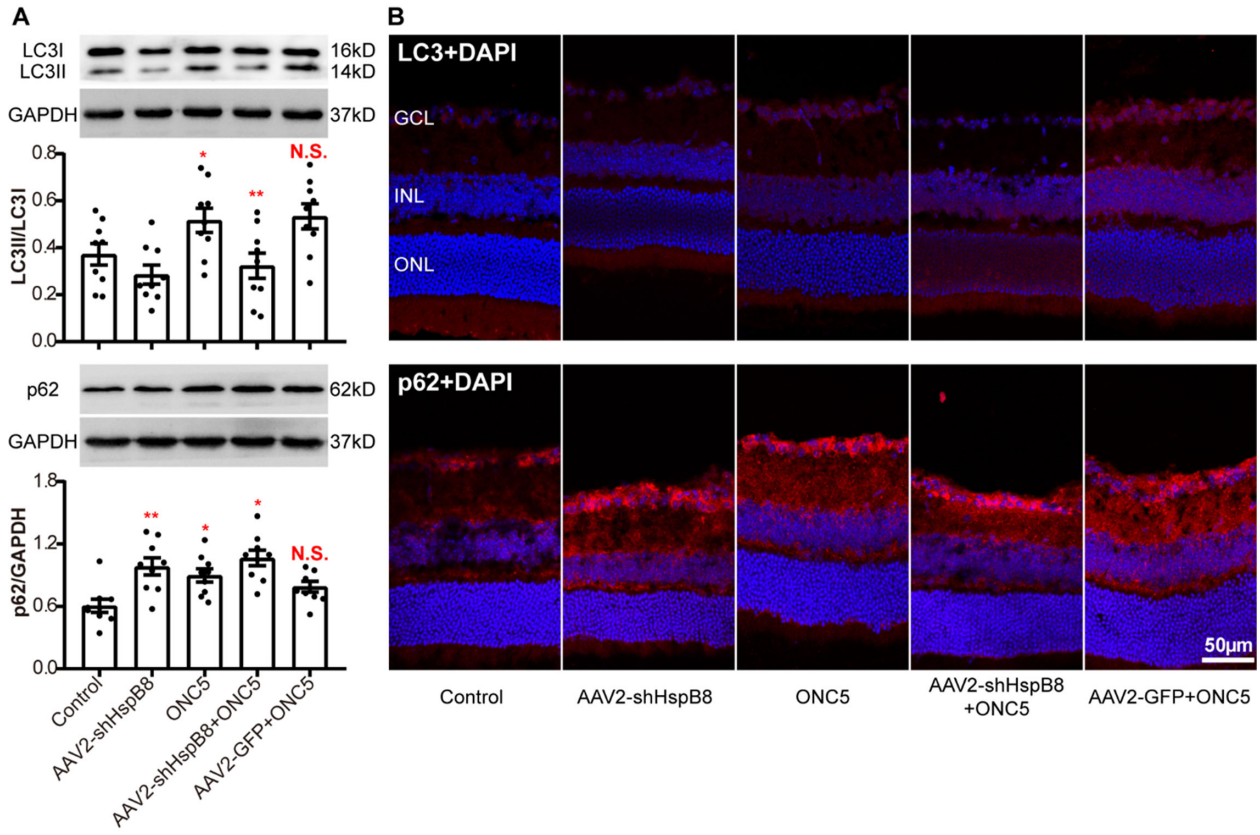

Figure 6. The ONC enhanced autophagy level was suppressed by AAV2-shHspB8. (**A**) For the LC3II/LC3I ratios for the AAV2-shHspB8 group (0.29 ± 0.04) compared with the control group (0.37 ± 0.05), $P = 0.2219$; for the ONC5 group (0.52 ± 0.05) compared with the control group, $P = 0.0444$; for the AAV2-shHspB8 + ONC5 group (0.32 ± 0.05) compared with the AAV2-GFP + ONC5 group (0.53 ± 0.05), $P = 0.0045$; and for the AAV2-GFP + ONC5 group compared with the ONC5 group, $P = 0.8111$. For the p62 levels for the AAV2-shHspB8 group (0.98 ± 0.08) compared with the control group (0.61 ± 0.06), $P = 0.0013$; for the ONC5 group (0.90 ± 0.06) compared with the control group, $P = 0.0170$; for the AAV2-shHspB8 + ONC5 group (1.07 ± 0.07) compared with the AAV2-GFP + ONC5 (0.79 ± 0.05) group, $P = 0.0260$; and for the AAV2-GFP + ONC5 group compared with the ONC5 group, $P = 0.7142$ ($n = 9$). All data are presented as mean ± SEM. (**B**) Immunofluorescent retinal sections of LC3 (*red*) and p62 (*red*); protein levels illustrated by fluorescence intensity in these five groups showed synchronized trends for the western blot results ($n = 3$).

intravitreal injection of AAV2 tends to transduce cells in the GCL,[32] our results show that HspB8 was distributed mainly in the GCL, thus laying a theoretical foundation for the subsequent intervention of HspB8 silencing and autophagy regulation in RGCs.

In this study, a decreased b-wave amplitude 5 days after ONC was observed, which can be explained by the possibility that ONC may mediate cell death in the INL and lead to b-wave impairment of ff-ERG. Research has proved that ON injury not only causes RGCs death but also leads to loss of neurons in the INL[33,34] and visual cortex,[35] axons of which do not reach into the ON. Furthermore, this functional change can also result from Müller cell activation induced by ON injury[36] and neurotrophic factors released from glial cells.[37]

Detection by ff-ERG also demonstrated that PhNR amplitudes were affected by ONC but OPs amplitudes were not, consistent with previous studies.[38,39] It is known that PhNRs originate from RGCs and reflect its visual electrophysiological performance,[40] and OPs are supposed to reflect the condition of retinal circulation.[41] Hence, we came to the conclusion that ONC causes dysfunction of RGCs without retinal circulation injury. In addition, asynchronism between RGCs death and visual acuity damage with regard to time and extent was exhibited in our study, which indicated that functional impairment was earlier and greater than RGCs death due to ON injury. Existing work has reported the same consequences and suggests that the remaining damaged axons are likely unable to continue transmitting visual signals.[42]

Numerous studies have confirmed that autophagy can be stimulated in RGCs after ON injury in terms of mRNA level, protein level, and ultrastructural characteristics.[18,29] An autophagy cascade is activated with significantly increased p62 levels 6 hours after acute axonal degeneration in the ON,[18] which may be caused by increased protein synthesis of p62 and insufficient autophagy flux and affected by levels of lysosomal-derived amino acids.[3,43] These theories would explain the raised p62 levels with activated autophagy by ONC in our study, as well.

Research findings suggest that autophagosomes increase rapidly and persistently as major components in the damaged ON, and this ultrastructural degeneration can be alleviated by intravitreal injection of 3MA.[18] The harmful effects of autophagy and neuroprotection of 3MA application in the soma of RGCs were also certified in our study. However, by using Atg4B and Atg5 knock-out mice, previous study shows that autophagy inhibition decreases cell

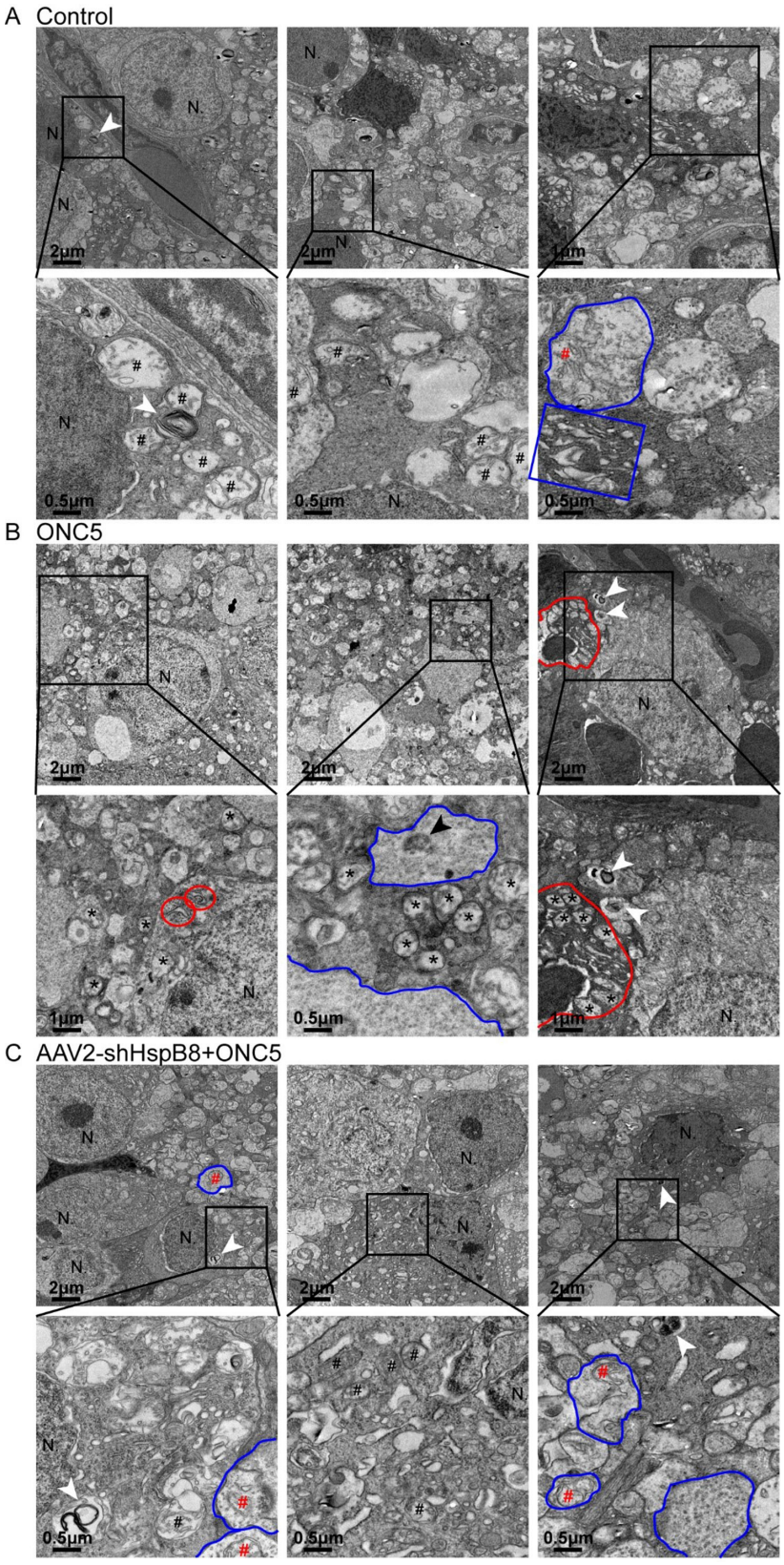

Figure 7. AAV2-shHspB8 inhibited autophagy and protected subcellular structures. N, nuclei of RGCs; *white arrowheads*, autolysosomes in the soma of RGCs; *black #*, normal mitochondria in the soma of RGCs; *red #*, normal mitochondria in nerve fibers; regions with *blue border*, unmyelinated nerve fibers and neurotubules inside; *blue rectangle*, normal Golgi apparatus and endoplasmic reticulum in the soma of RGCs; region with *red border*, apoptosis RGCs and its pyknotic nucleus; *red circles*, vesicular expansions of the endoplasmic reticulum; *black arrowhead*, autophagosome in nerve fiber. *Swollen or vacuolar mitochondria.

Investigative Ophthalmology & Visual Science

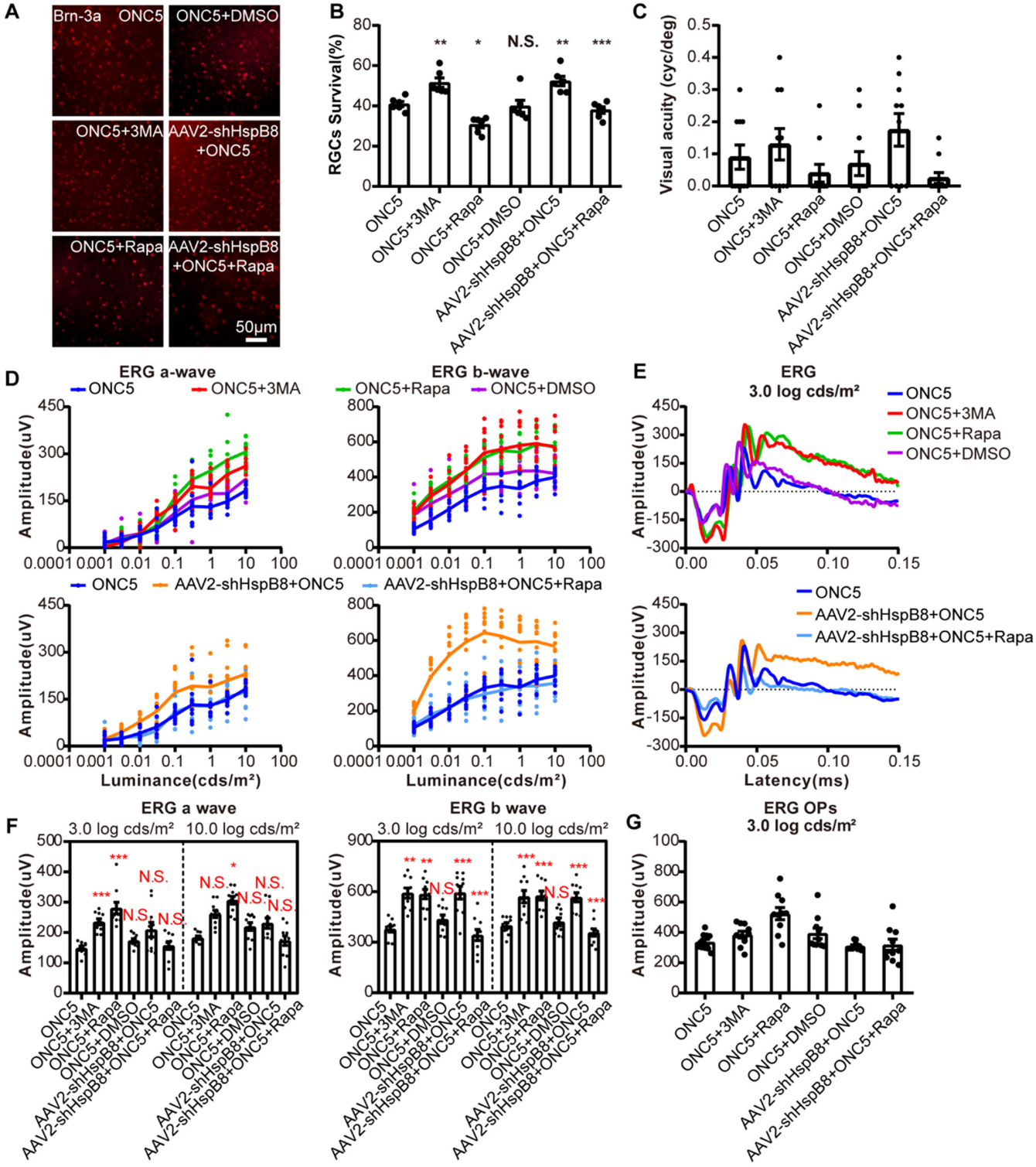

Figure 8. AAV2-shHspB8 played a neuroprotective role by inhibiting autophagy. (**A**) Representative images of RGCs immunofluorescent staining (Brn3a). (**B**) For the ONC5-3MA group (51.53% ± 2.39%) compared with the ONC5-DMSO group (39.82% ± 2.92%), $P = 0.0024$; for the ONC5-Rapa group (30.71% ± 1.62%) compared with the ONC5-DMSO group, $P = 0.0238$; for the ONC5 group (40.93% ± 1.32%) compared with the ONC5-DMSO group, $P = 0.9981$; for the ONC5 group compared with the AAV2-shHspB8 + ONC5 group (52.32% ± 2.38%), $P = 0.0032$; for the AAV2-shHspB8 + ONC5 + Rapa group (37.95% ± 1.62%) compared with the AAV2-shHspB8 + ONC5 group, $P = 0.0002$ ($n = 6$). (**C**) Visual acuity in the OMR test ($n = 10$). (**D**) The a- and b-wave amplitudes under different flash light intensions ($n = 10$). (**E**) Example ERG waves at 3.0 cd·s/m^2. (**F**) The a-wave amplitudes at 3.0 and 10.0 cd·s/m^2 and b-wave amplitudes at 3.0 and 10.0 cd·s/m^2: for the ONC5-3MA group compared with the ONC5-DMSO group, $P = 0.0004$, $P = 0.4801$, $P = 0.0021$, and $P = 0.0008$, respectively; for the ONC5-Rapa group compared with the ONC5-DMSO group, $P = 0.0012$, $P = 0.0198$, $P = 0.0034$, and $P = 0.0004$, respectively; for the ONC5 group compared with the ONC5-DMSO group, $P = 0.0733$, $P = 0.3971$, $P = 0.5879$, and $P = 0.9839$, respectively; for the ONC5 group compared with the AAV2-shHspB8 + ONC5 group, $P = 0.1531$, $P = 0.2154$, $P < 0.0001$, and $P = 0.0002$, respectively; and for the AAV2-shHspB8 + ONC5 + Rapa group compared with the AAV2-shHspB8 + ONC5 group, $P = 0.3198$, $P = 0.2154$, $P < 0.0001$, and $P < 0.0001$, respectively ($n = 10$). Data are shown in the Table. (**G**) Amplitudes of OPs at 3.0 cd·s/m^2 ($n = 10$). Data are shown in the Table.

Investigative Ophthalmology & Visual Science

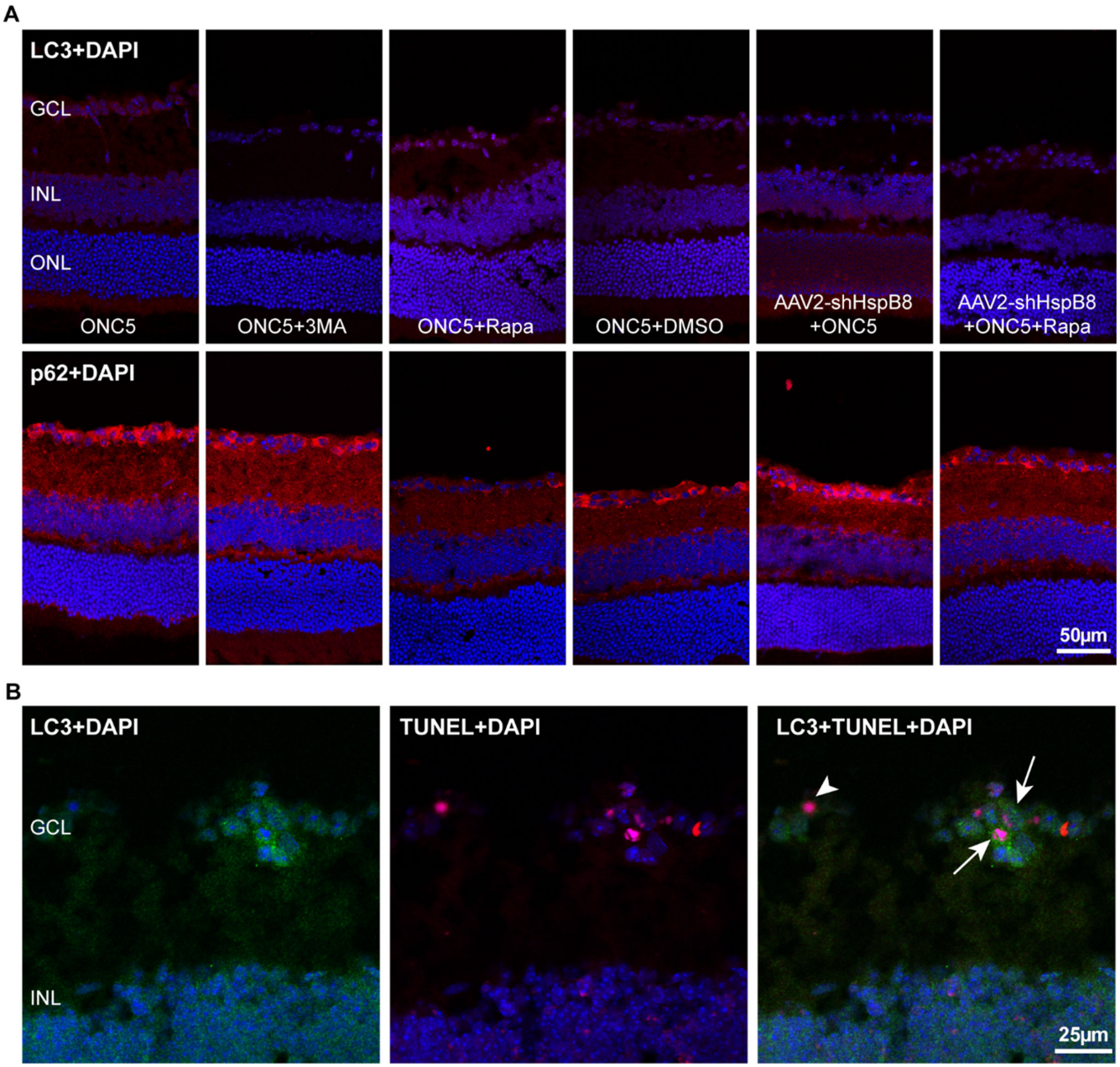

Figure 9. Immunofluorescent evidence of autophagy level after intervention and the relationship between autophagy and apoptosis in RGCs. (**A**) Retinal slices stained with LC3 (*red*), p62 (*red*), and DAPI (*blue*) ($n = 3$). (**B**) Multiple staining of LC3 (*green*), TUNEL (*red*), and DAPI (*blue*) in retinal sections of the ONC5 group.

viability while Rapa increases cell survival in RGCs after ON transection.[28] There is a narrow therapeutic window for autophagy to affect RGCs survival rates and axonal integrity,[3] and autophagy has a wide range of effects from neuroprotection to neurodegeneration.[19,44,45] We suggest that the requirements for autophagy vary with physiological states and regions of neurocytes, which may lead to different consequences of autophagy activation. Therefore, we have reason to infer that these controversial results can be due to the multiple effects of gene knockout type and varying animal models, species, and examination times. These seemingly contradictory results suggest a critical role of autophagy in maintaining axonal homeostasis, so we should pay attention to the timing of intervention and carry out dynamic treatment, because inappropriate manipulation of autophagy may turn the double-edged sword onto its other side.

HspB8 combines with BAG3 to form a complex that is involved in the regulation of macroautophagy.[46,47] This complex recruits Hsp70 and then mediates the chaperone-assisted selective autophagy.[9,48] Previous studies have reported that HspB8 promotes the fusion of autophagosome and lysosome during autophagy,[49] whereas the HspB8 K141E mutation impairs this fusion.[50] These results suggest that HspB8 stimulated the forming process instead of the degradation of autophagosomes. This perspective is also supported by our observation that AAV2-shHspB8 had the same neuroprotective impacts as 3MA in ONC, since 3MA is

Investigative Ophthalmology & Visual Science

known as a PI3K inhibitor and can block the formation of autophagosomes.[51,52]

It has been suggested that nuclear factor kappa B (NF-κB), one of the best known regulators of HSPB8 and BAG3, influences the expression of HspB8.[53,54] It has been found to be activated by p62 through the receptor activator of nuclear factor κ B (RANK)–p62–tumor necrosis factor receptor (TNFR)-associated factor 6 (TRAF6)–NF-κB pathway.[55,56] Knowing that HspB8 can regulate autophagy level and thus indirectly affect the expression of p62, we can make the reasonable assumption that there is a mutual influence between HspB8 and the RANK–p62–TRAF6–NF-κB axis. The dynamic change of HspB8 protein level after ONC in this study may be explained by this hypothesis.

Currently, the interactions and interdependencies among the HSPs in neuronal diseases have not been well studied. Several studies have considered the protective roles of HSP70 and HSP90 in RGCs death.[57,58] We found that excess HspB8 was a detriment after RGCs damage. HSP27, belonging to the same HspBs family as HspB8, is speculated to be involved in the induction of neuroinflammation in an autoimmune glaucoma model.[59] These seemingly contradictory consequences may due to the varying physiological properties of different HSP groups. HSPA (HSP70) family members bind to misfolded proteins and lead to its refolding. The HSPC (HSP90) family is essential for proper folding, activation, and stabilization of client proteins, and HspBs insulate proteins and prevent their aggregation.[60] However, protein quality control is a very complicated system, different intervened components may ultimately result in variable conditions.

In conclusion, our results demonstrate the neuroprotection of AAV2-shHspB8 through autophagy suppression in mice ON injury and provide a possible direction for further scientific exploration and neuroprotective treatment for axonal degeneration. Future researchers could focus on the deeper mechanisms of HspB8 and autophagy in the visual system, as well as the relationship between HspB8 and the RANK–p62–TRAF6–NF-κB axis.

Acknowledgments

The authors thank Ying Li, Xinlan Lei, Qinqin Deng, Ning Ma, and Xiao Zhang for their excellent and constructive suggestions.

Supported by grants from the National Natural Science Foundation of China (81271025), Natural Science Foundation of Hubei Province (2020CFB240), and Fundamental Research Funds for the Central Universities (2042020kf0065).

Disclosure: **F. Xie**, None; **Z. Li**, None; **N. Yang**, None; **J. Yang**, None; **D. Hua**, None; **J. Luo**, None; **T. He**, None; **Y. Xing**, None

References

1. Planchamp V, Bermel C, Tonges L, et al. BAG1 promotes axonal outgrowth and regeneration *in vivo* via Raf-1 and reduction of ROCK activity. *Brain*. 2008;131(pt 10):2606–2619.
2. Wang XW, Li Q, Liu CM, et al. Lin28 signaling supports mammalian PNS and CNS axon regeneration. *Cell Rep*. 2018;24(10):2540–2552.e2546.
3. Koch JC, Lingor P. The role of autophagy in axonal degeneration of the optic nerve. *Exp Eye Res*. 2016;144:81–89.
4. Lambiase A, Aloe L, Centofanti M, et al. Experimental and clinical evidence of neuroprotection by nerve growth factor eye drops: implications for glaucoma. *Proc Natl Acad Sci USA*. 2009;106(32):13469–13474.
5. Mac Nair CE, Fernandes KA, Schlamp CL, Libby RT, Nickells RW. Tumor necrosis factor alpha has an early protective effect on retinal ganglion cells after optic nerve crush. *J Neuroinflammation*. 2014;11:194.
6. Sanchez-Migallon MC, Valiente-Soriano FJ, Nadal-Nicolas FM, Vidal-Sanz M, Agudo-Barriuso M. Apoptotic retinal ganglion cell death after optic nerve transection or crush in mice: delayed RGCs loss with BDNF or a caspase 3 inhibitor. *Invest Ophthalmol Vis Sci*. 2016;57(1):81–93.
7. Li HY, Ruan YW, Ren CR, Cui Q, So KF. Mechanisms of secondary degeneration after partial optic nerve transection. *Neural Regen Res*. 2014;9(6):565–574.
8. Haslbeck M, Franzmann T, Weinfurtner D, Buchner J. Some like it hot: the structure and function of small heat-shock proteins. *Nat Struct Mol Biol*. 2005;12(10):842–846.
9. Carra S, Seguin SJ, Landry J. HspB8 and Bag3: a new chaperone complex targeting misfolded proteins to macroautophagy. *Autophagy*. 2008;4(2):237–239.
10. Shemetov AA, Gusev NB. Biochemical characterization of small heat shock protein HspB8 (Hsp22)–Bag3 interaction. *Arch Biochem Biophys*. 2011;513(1):1–9.
11. Carra S, Seguin SJ, Lambert H, Landry J HspB8 chaperone activity toward poly(Q)-containing proteins depends on its association with Bag3, a stimulator of macroautophagy. *J Biol Chem*. 2008;283(3):1437–1444.
12. Seidel K, Vinet J, Dunnen WF, et al. The HSPB8-BAG3 chaperone complex is upregulated in astrocytes in the human brain affected by protein aggregation diseases. *Neuropathol Appl Neurobiol*. 2012;38(1):39–53.
13. Li F, Tan J, Zhou F, Hu Z, Yang B. Heat shock protein B8 (HSPB8) reduces oxygen-glucose deprivation/reperfusion injury via the induction of mitophagy. *Cell Physiol Biochem*. 2018;48(4):1492–1504.
14. Hase M, Depre C, Vatner SF, Sadoshima J. H11 has dose-dependent and dual hypertrophic and proapoptotic functions in cardiac myocytes. *Biochem J*. 2005;388(pt 2):475–483.
15. Acunzo J, Katsogiannou M, Rocchi P. Small heat shock proteins HSP27 (HspB1), alphaB-crystallin (HspB5) and HSP22 (HspB8) as regulators of cell death. *Int J Biochem Cell Biol*. 2012;44(10):1622–1631.
16. Boya P, Reggiori F, Codogno P. Emerging regulation and functions of autophagy. *Nat Cell Biol*. 2013;15(7):713–720.
17. Boya P, Esteban-Martinez L, Serrano-Puebla A, Gomez-Sintes R, Villarejo-Zori B. Autophagy in the eye: development, degeneration, and aging. *Prog Retin Eye Res*. 2016;55:206–245.
18. Knoferle J, Koch JC, Ostendorf T, et al. Mechanisms of acute axonal degeneration in the optic nerve in vivo. *Proc Natl Acad Sci USA*. 2010;107(13):6064–6069.
19. Rodriguez-Muela N, Boya P. Axonal damage, autophagy and neuronal survival. *Autophagy*. 2012;8(2):286–288.
20. Luo J, He T, Yang J, Yang N, Li Z, Xing Y. SIRT1 is required for the neuroprotection of resveratrol on retinal ganglion cells after retinal ischemia-reperfusion injury in mice. *Graefes Arch Clin Exp Ophthalmol*. 2020;258(2):335–344.
21. Yang J, Yang N, Luo J, et al. Overexpression of S100A4 protects retinal ganglion cells against retinal ischemia-reperfusion injury in mice. *Exp Eye Res*. 2020;201:108281.
22. Zhang B, Yin X, Li J, et al. Essential contribution of macrophage Tie2 signal mediated autophagy in laser-induced choroidal neovascularization. *Exp Eye Res*. 2020;193:107972.
23. Kitaoka Y, Munemasa Y, Kojima K, Hirano A, Ueno S, Takagi H. Axonal protection by Nmnat3 overexpression with involvement of autophagy in optic nerve degeneration. *Cell Death Dis*. 2013;4:e860.

24. Prusky GT, Alam NM, Beekman S, Douglas RM. Rapid quantification of adult and developing mouse spatial vision using a virtual optomotor system. *Invest Ophthalmol Vis Sci*. 2004;45(12):4611–4616.
25. Yang N, Zhang W, He T, Xing Y. Silencing of galectin-1 inhibits retinal neovascularization and ameliorates retinal hypoxia in a murine model of oxygen-induced ischemic retinopathy. *Exp Eye Res*. 2017;159:1–15.
26. Kabeya Y, Mizushima N, Ueno T, et al. LC3, a mammalian homologue of yeast Apg8p, is localized in autophagosome membranes after processing. *EMBO J*. 2000;19(21):5720–5728.
27. Moscat J, Diaz-Meco MT. p62 at the crossroads of autophagy, apoptosis, and cancer. *Cell*. 2009;137(6):1001–1004.
28. Rodriguez-Muela N, Germain F, Marino G, Fitze PS, Boya P. Autophagy promotes survival of retinal ganglion cells after optic nerve axotomy in mice. *Cell Death Differ*. 2012;19(1):162–169.
29. Kim SH, Munemasa Y, Kwong JM, et al. Activation of autophagy in retinal ganglion cells. *J Neurosci Res*. 2008;86(13):2943–2951.
30. Maday S. Mechanisms of neuronal homeostasis: autophagy in the axon. *Brain Res*. 2016;1649(pt B):143–150.
31. Kang LH, Zhang S, Jiang S, Hu N. Activation of autophagy in the retina after optic nerve crush injury in rats. *Int J Ophthalmol*. 2019;12(9):1395–1401.
32. Giove TJ, Sena-Esteves M, Eldred WD. Transduction of the inner mouse retina using AAVrh8 and AAVrh10 via intravitreal injection. *Exp Eye Res*. 2010;91(5):652–659.
33. Rey-Funes M, Larrayoz IM, Contartese DS, et al. Hypothermia prevents retinal damage generated by optic nerve trauma in the rat. *Sci Rep*. 2017;7(1):6966.
34. Shen Y, Luo X, Liu S, Shen Y, Nawy S, Shen Y. Rod bipolar cells dysfunction occurs before ganglion cells loss in excitotoxin-damaged mouse retina. *Cell Death Dis*. 2019;10(12):905.
35. Liu Y, McDowell CM, Zhang Z, Tebow HE, Wordinger RJ, Clark AF. Monitoring retinal morphologic and functional changes in mice following optic nerve crush. *Invest Ophthalmol Vis Sci*. 2014;55(6):3766–3774.
36. Casson RJ, Chidlow G, Wood JP, Vidal-Sanz M, Osborne NN. The effect of retinal ganglion cell injury on light-induced photoreceptor degeneration. *Invest Ophthalmol Vis Sci*. 2004;45(2):685–693.
37. Alarcon-Martinez L, de la Villa P, Aviles-Trigueros M, Blanco R, Villegas-Perez MP, Vidal-Sanz M. Short and long term axotomy-induced ERG changes in albino and pigmented rats. *Mol Vis*. 2009;15:2373–2383.
38. Bui BV, Fortune B. Ganglion cell contributions to the rat full-field electroretinogram. *J Physiol*. 2004;555(pt 1):153–173.
39. Li B, Barnes GE, Holt WF. The decline of the photopic negative response (PhNR) in the rat after optic nerve transection. *Doc Ophthalmol*. 2005;111(1):23–31.
40. Bhatti T, Tariq A, Shen T, Williams KM, Hammond CJ, Mahroo OA. Relative genetic and environmental contributions to variations in human retinal electrical responses quantified in a twin study. *Ophthalmology*. 2017;124(8):1175–1185.
41. Tsai SH, Xie W, Zhao M, Rosa RH, Jr, Hein TW, Kuo L. Alterations of ocular hemodynamics impair ophthalmic vascular and neuroretinal function. *Am J Pathol*. 2018;188(3):818–827.
42. Grinblat GA, Khan RS, Dine K, Wessel H, Brown L, Shindler KS. RGCs neuroprotection following optic nerve trauma mediated by intranasal delivery of amnion cell secretome. *Invest Ophthalmol Vis Sci*. 2018;59(6):2470–2477.
43. Sahani MH, Itakura E, Mizushima N. Expression of the autophagy substrate SQSTM1/p62 is restored during prolonged starvation depending on transcriptional upregulation and autophagy-derived amino acids. *Autophagy*. 2014;10(3):431–441.
44. Jaeger PA, Wyss-Coray T. All-you-can-eat: autophagy in neurodegeneration and neuroprotection. *Mol Neurodegener*. 2009;4:16.
45. Galluzzi L, Vicencio JM, Kepp O, Tasdemir E, Maiuri MC, Kroemer G. To die or not to die: that is the autophagic question. *Curr Mol Med*. 2008;8(2):78–91.
46. Carra S, Brunsting JF, Lambert H, Landry J, Kampinga HH. HspB8 participates in protein quality control by a non-chaperone-like mechanism that requires eIF2{alpha} phosphorylation. *J Biol Chem*. 2009;284(9):5523–5532.
47. Carra S. The stress-inducible HspB8-Bag3 complex induces the eIF2alpha kinase pathway: implications for protein quality control and viral factory degradation? *Autophagy*. 2009;5(3):428–429.
48. Arndt V, Dick N, Tawo R, et al. Chaperone-assisted selective autophagy is essential for muscle maintenance. *Curr Biol*. 2010;20(2):143–148.
49. Li XC, Hu QK, Chen L, et al. HSPB8 promotes the fusion of autophagosome and lysosome during autophagy in diabetic neurons. *Int J Med Sci*. 2017;14(13):1335–1341.
50. Kwok AS, Phadwal K, Turner BJ, et al. HspB8 mutation causing hereditary distal motor neuropathy impairs lysosomal delivery of autophagosomes. *J Neurochem*. 2011;119(6):1155–1161.
51. Hou H, Zhang Y, Huang Y, et al. Inhibitors of phosphatidylinositol 3′-kinases promote mitotic cell death in HeLa cells. *PLoS One*. 2012;7(4):e35665.
52. Seglen PO, Gordon PB. 3-Methyladenine: specific inhibitor of autophagic/lysosomal protein degradation in isolated rat hepatocytes. *Proc Natl Acad Sci USA*. 1982;79(6):1889–1892.
53. Cristofani R, Rusmini P, Galbiati M, et al. The regulation of the small heat shock protein b8 in misfolding protein diseases causing motoneuronal and muscle cell death. *Front Neurosci*. 2019;13:796.
54. Nivon M, Abou-Samra M, Richet E, Guyot B, Arrigo AP, Kretz-Remy C. NF-κB regulates protein quality control after heat stress through modulation of the BAG3–HspB8 complex. *J Cell Sci*. 2012;125(pt 5):1141–1151.
55. Sanz L, Diaz-Meco MT, Nakano H, Moscat J. The atypical PKC-interacting protein p62 channels NF-κB activation by the IL-1–TRAF6 pathway. *EMBO J*. 2000;19(7):1576–1586.
56. Moscat J, Diaz-Meco MT, Albert A, Campuzano S. Cell signaling and function organized by PB1 domain interactions. *Mol Cell*. 2006;23(5):631–640.
57. Biermann J, Lagreze WA, Dimitriu C, Stoykow C, Goebel U. Preconditioning with inhalative carbon monoxide protects rat retinal ganglion cells from ischemia/reperfusion injury. *Invest Ophthalmol Vis Sci*. 2010;51(7):3784–3791.
58. Biermann J, Lagreze WA, Schallner N, Schwer CI, Goebel U. Inhalative preconditioning with hydrogen sulfide attenuated apoptosis after retinal ischemia/reperfusion injury. *Mol Vis*. 2011;17:1275–1286.
59. Casola C, Reinehr S, Kuehn S, et al. Specific inner retinal layer cell damage in an autoimmune glaucoma model is induced by GDNF with or without HSP27. *Invest Ophthalmol Vis Sci*. 2016;57(8):3626–3639.
60. Penke B, Bogar F, Crul T, Santha M, Toth ME, Vigh L. Heat shock proteins and autophagy pathways in neuroprotection: from molecular bases to pharmacological interventions. *Int J Mol Sci*. 2018;19(1):325.

Investigative Ophthalmology & Visual Science